

Supporting Information for

**Carbon Quantum Dots in Ionic Liquids: A New Generation of
Environmentally-Benign Photoluminescent Ink**

*Xiaofeng Sun, Keyang Yin, Baoyong Liu, Shengju Zhou, Jiamei Cao, Geping Zhang, and
Hongguang Li**

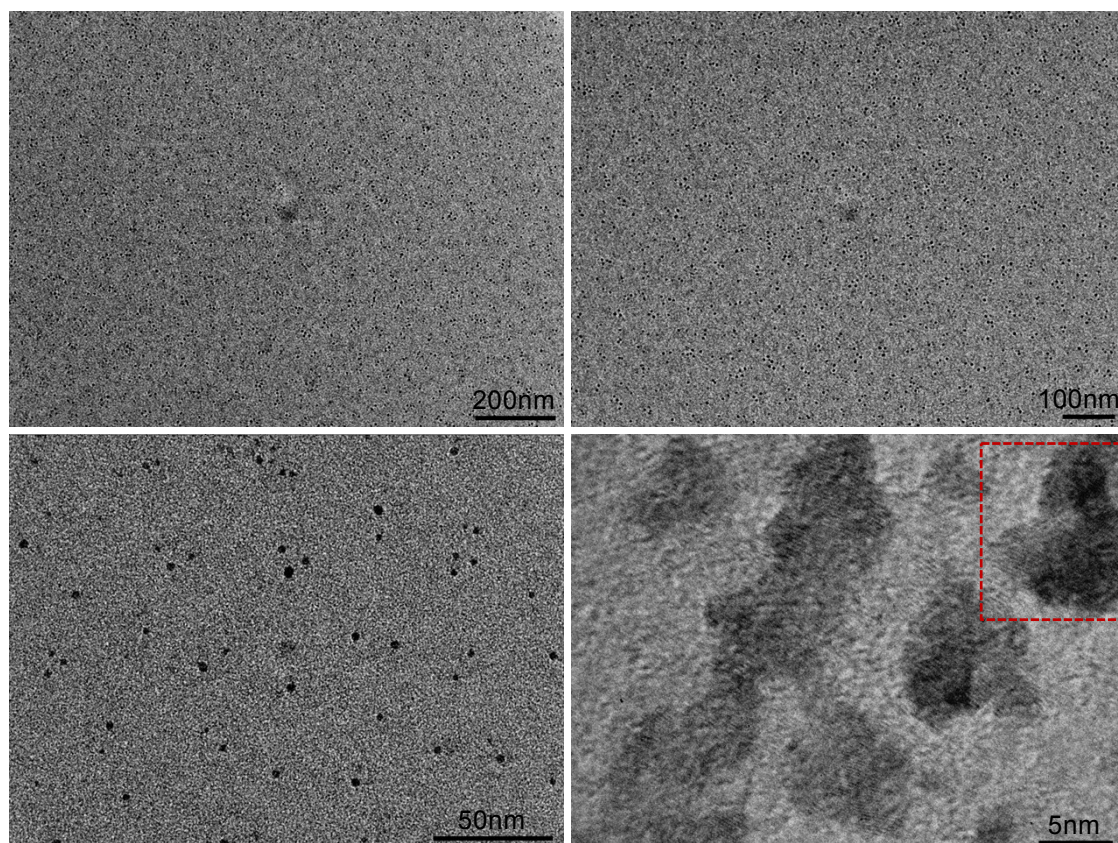


Fig. S1 HRTEM images at different magnifications of as-prepared Imi-CQDs-Br. The square in the last image denotes image b shown in Fig. 1 in the maintext.

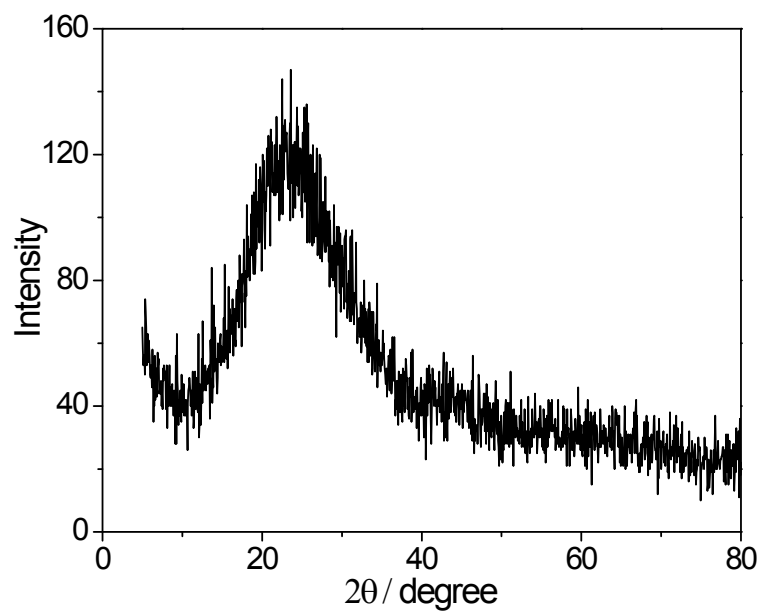


Fig. S2 XRD pattern of as-prepared Imi-CQDs-Br.

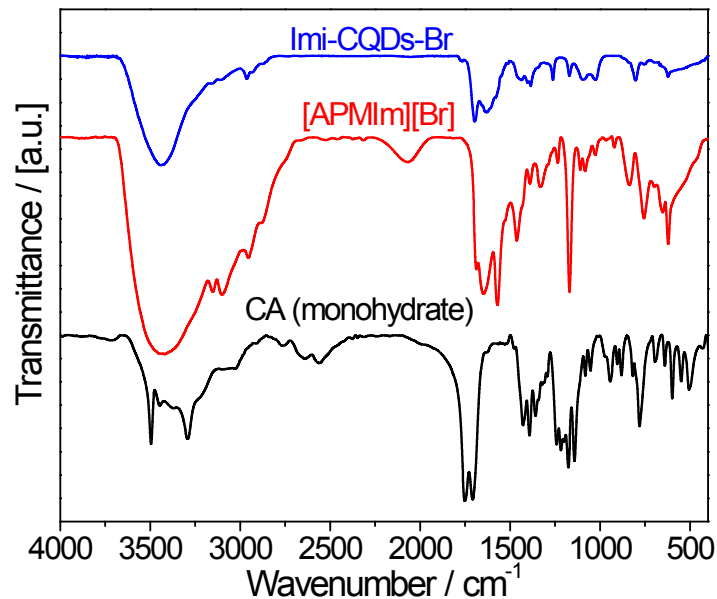


Fig. S3 FTIR spectra of CA (monohydrate), [APMIm][Br] and as-prepared Imi-CQDs-Br.

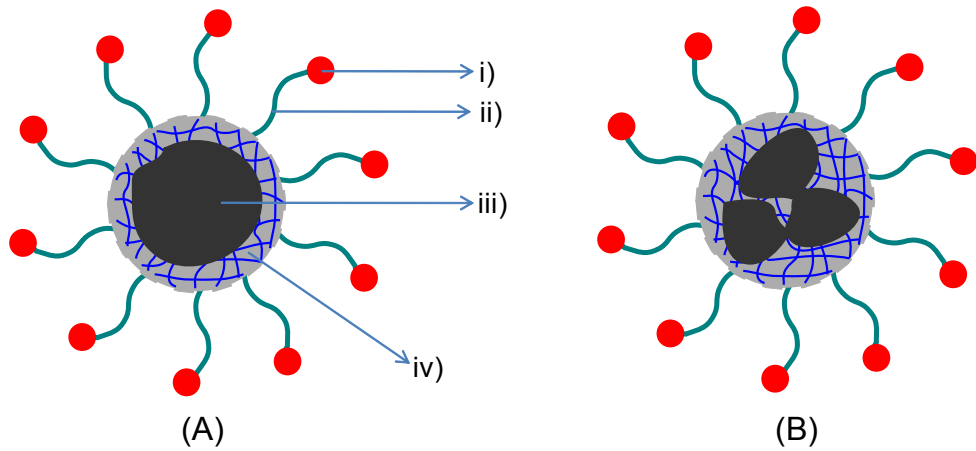


Fig. S4 In current pyrolysis condition, some of CA molecules may be only condensed to form organic networks connecting or surrounding the cores, as illustrated here. A gives a carbon quantum dot which contains one solid core, while B represents the case containing multiple cores. i) The imidazolium moiety; ii) the linker; iii) solid core produced by the complete pyrolysis of CA; iv) the polymeric network from incomplete pyrolysis of CA.

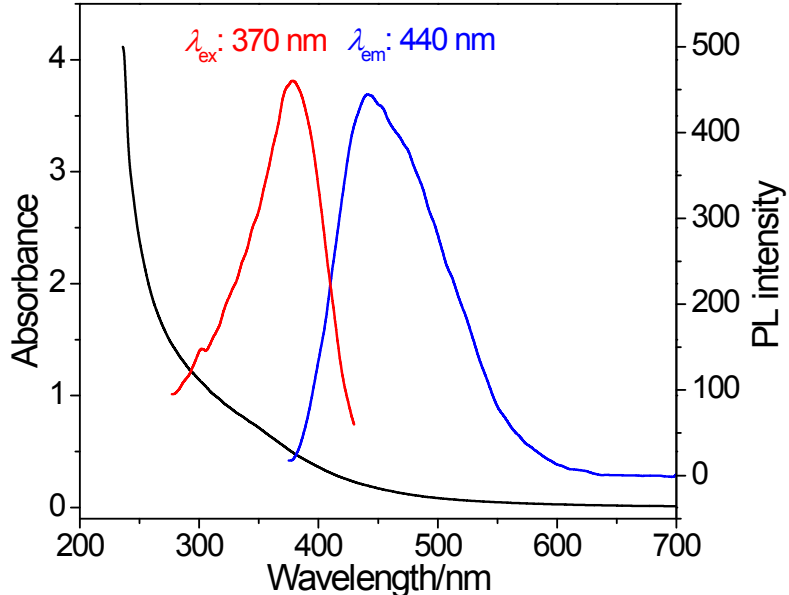


Fig. S5 UV-vis absorbance, the optimal λ_{ex} and λ_{em} of an aqueous solution of as-prepared Imi-CQDs-Br (0.5 mg·mL⁻¹).

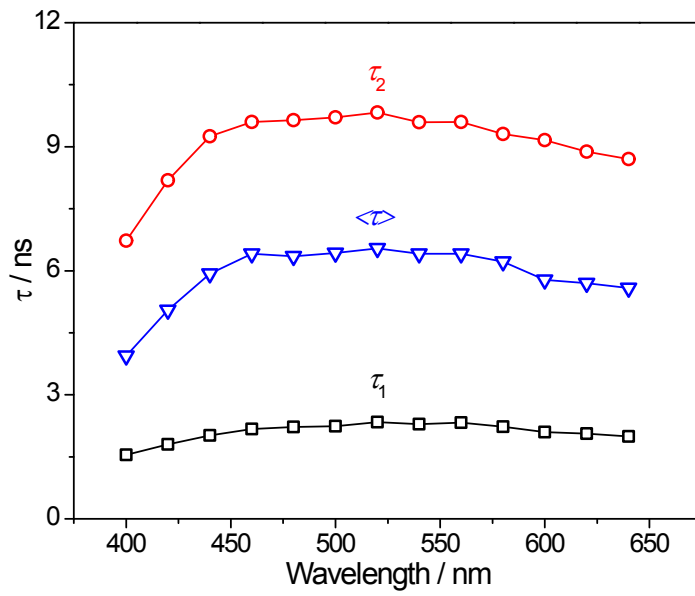


Fig. S6 Variations of τ_1 , τ_2 , and $\langle \tau \rangle$ as a function of emission wavelength for an aqueous solution of as-prepared Imi-CQDs-Br in water ($0.5 \text{ mg}\cdot\text{mL}^{-1}$, $\lambda_{\text{ex}} = 377.8 \text{ nm}$).

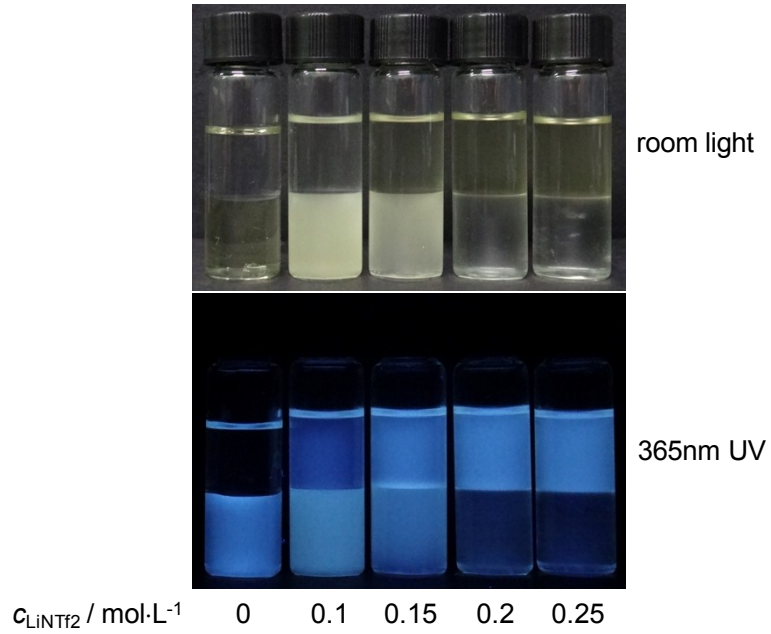


Fig. S7 Photos of aqueous Imi-CQDs-Br (bottom phase)/EA (upper phase) biphasic system, denoting the transfer of Imi-CQDs⁺ from the bottom aqueous phase to the upper EA phase triggered by the continuously addition of LiNTf₂. The concentration of Imi-CQDs-Br is fixed at $0.5 \text{ mg}\cdot\text{mL}^{-1}$.

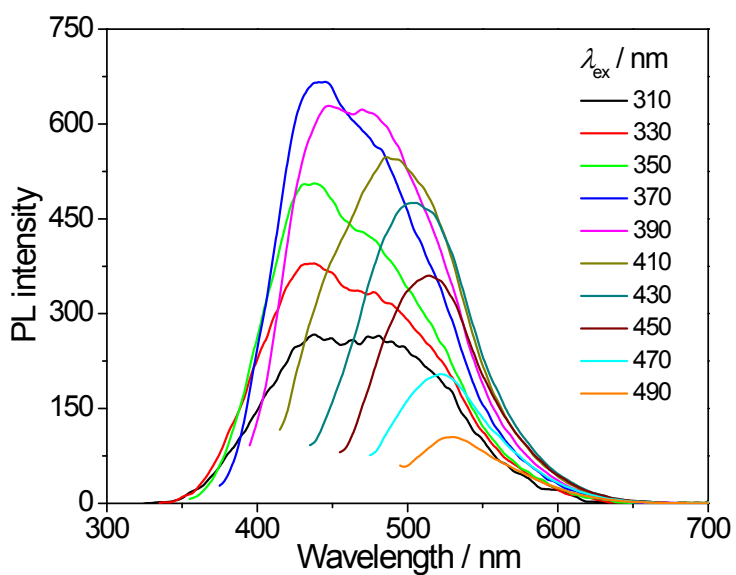


Fig. S8 Wavelength-dependent PL properties of Imi-CQDs-NTf₂ in EA after phase transfer.

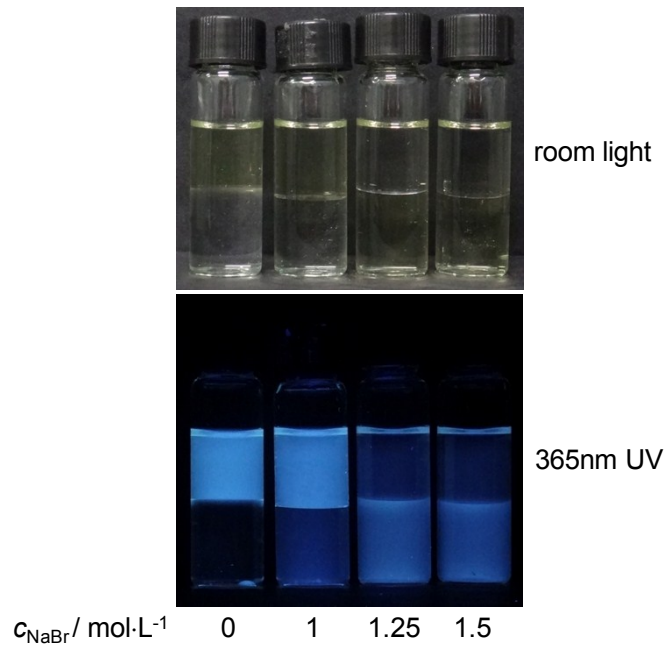


Fig. S9 Photos of Imi-CQDs-NTf₂ in EA (upper phase)/water (bottom phase) biphasic system, denoting the transfer of Imi-CQDs⁺ from the upper EA phase to the bottom aqueous phase triggered by the continuously addition of NaBr.

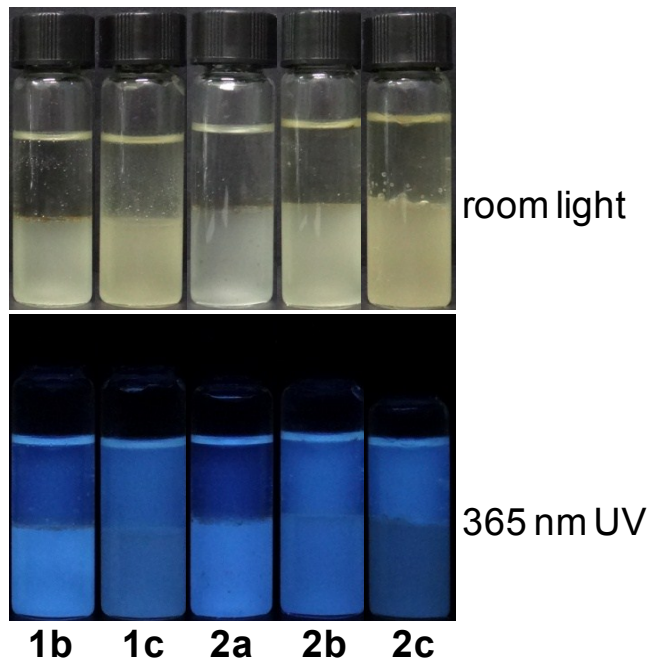


Fig. S10 Phase transfer of Imi-CQDs⁺ between water and RTILs with different structures.

$$c_{\text{Imi-CQDs-Br}} = 0.5 \text{ mg}\cdot\text{mL}^{-1}$$

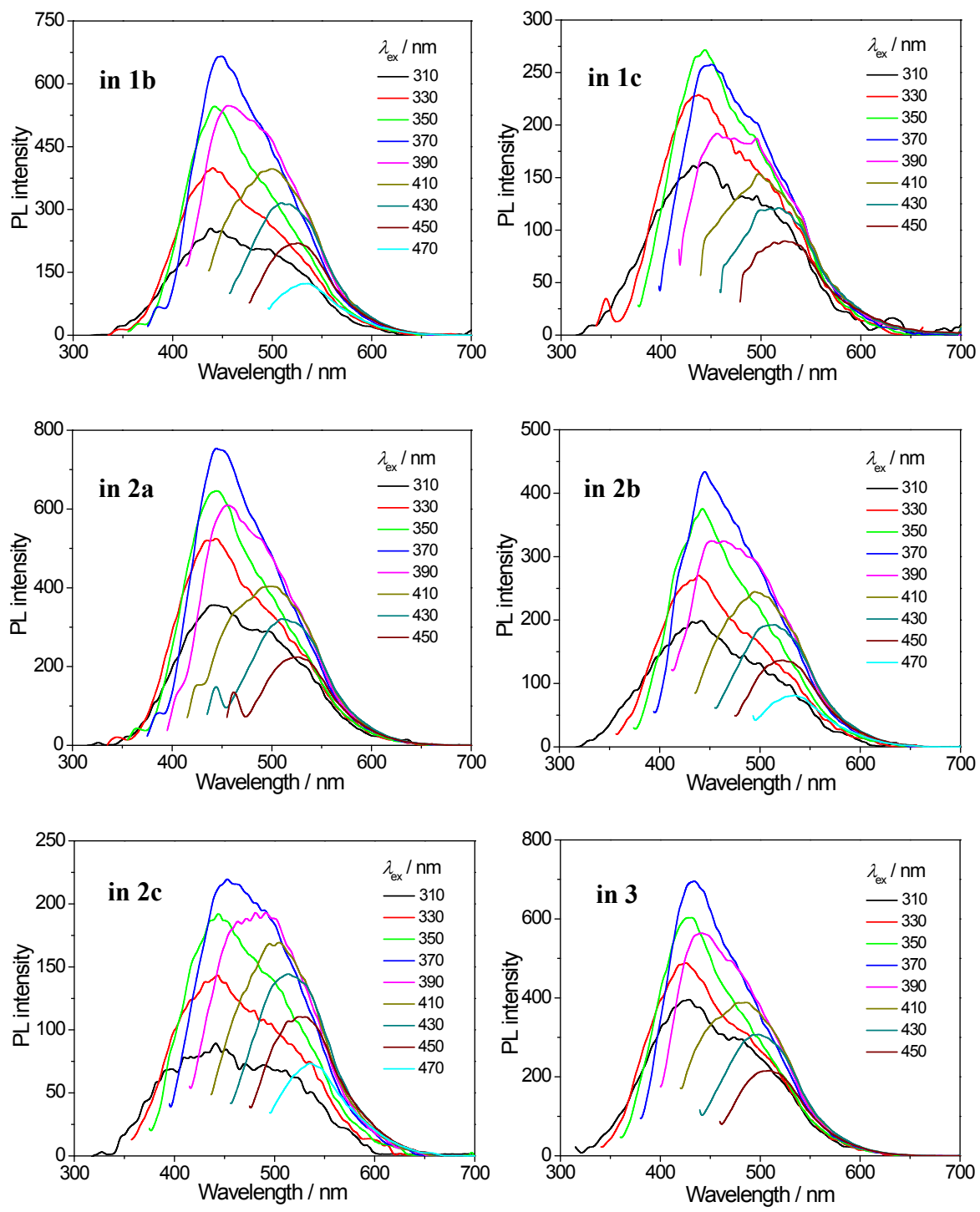


Fig. S11 PL properties at different λ_{ex} of Imi-CQDs⁺ in various RTILs as indicated.

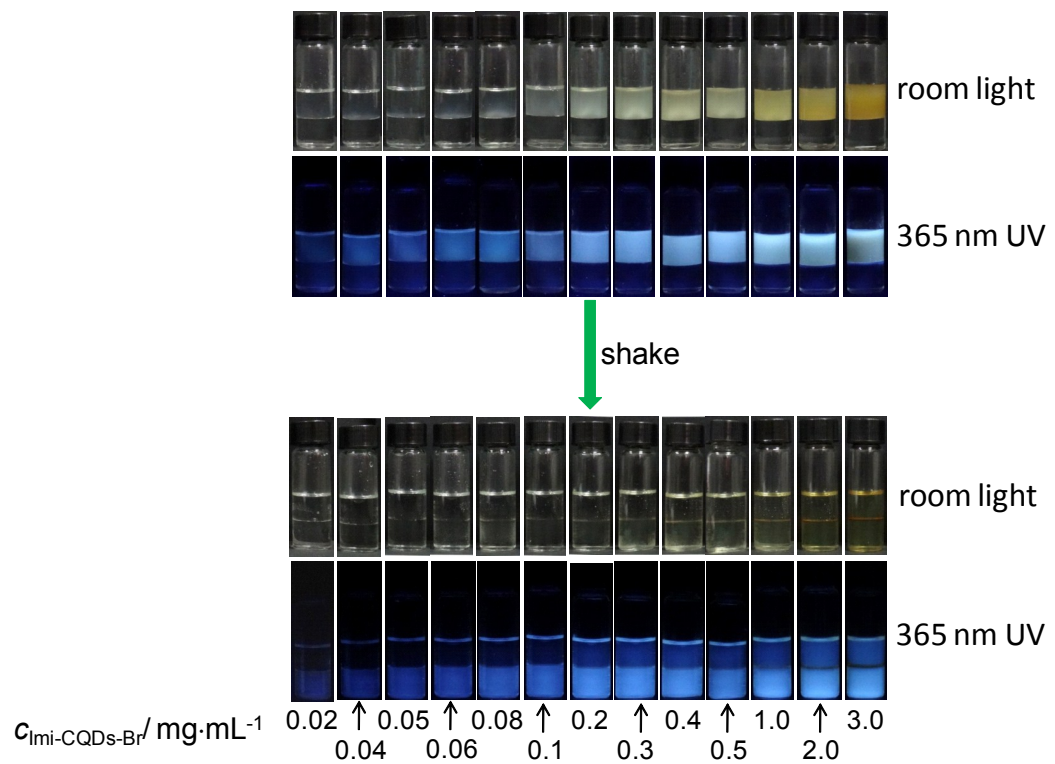


Fig. S12 Phase transfer between water and **1a** at different initial $c_{\text{Imi-CQDs-Br}}$ as indicated.

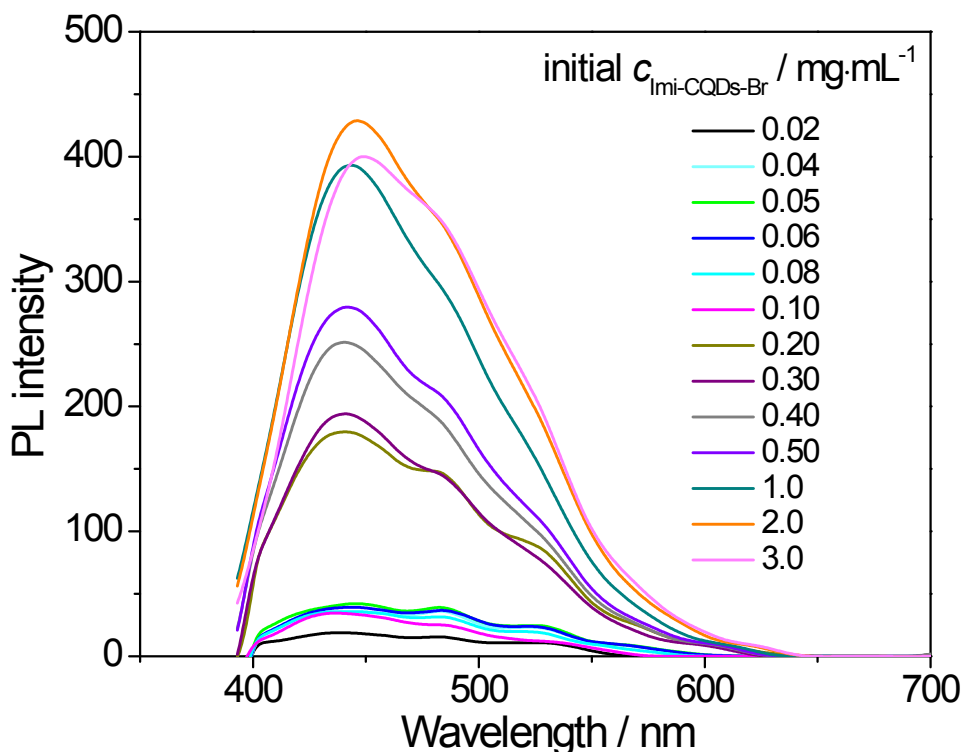


Fig. S13 PL spectra of Imi-CQDs-Br in water after phase transfer for the series samples shown in Fig. S12.

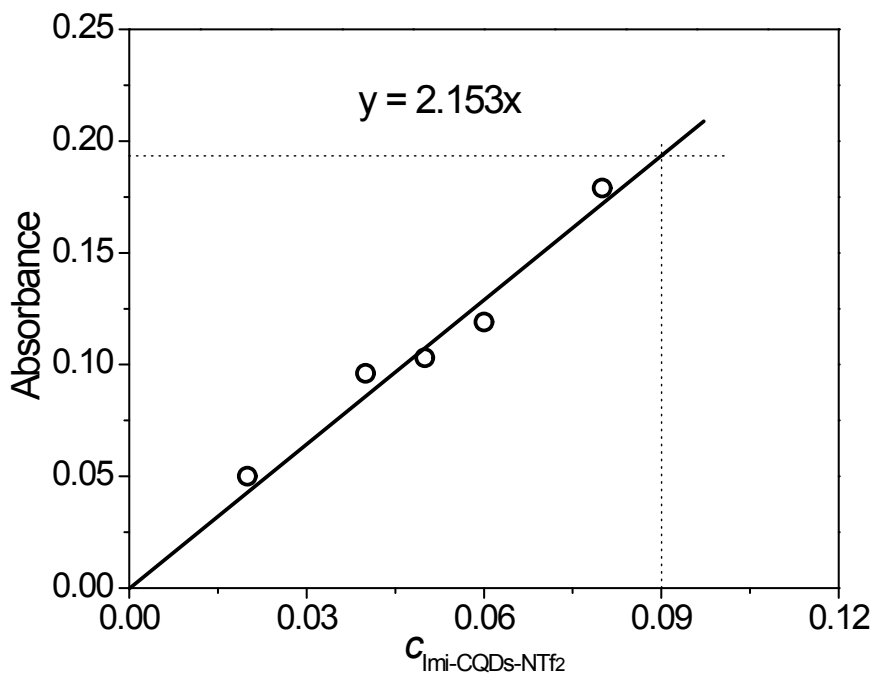


Fig. S14 UV-vis absorbance at 300 nm of Imi-CQDs-NTf₂ in **1a** after phase transfer at concentrations of < 0.1 mg·mL⁻¹.

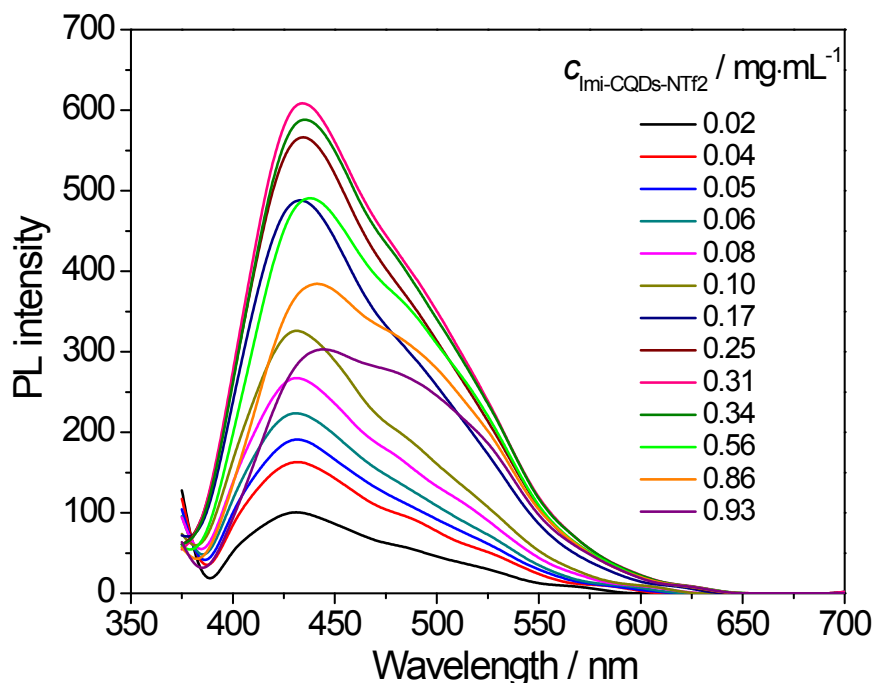


Fig. S15 Concentration-dependent photoluminescence of Imi-CQDs-NTf₂ in **1a** at $\lambda_{\text{ex}} = 370$ nm.

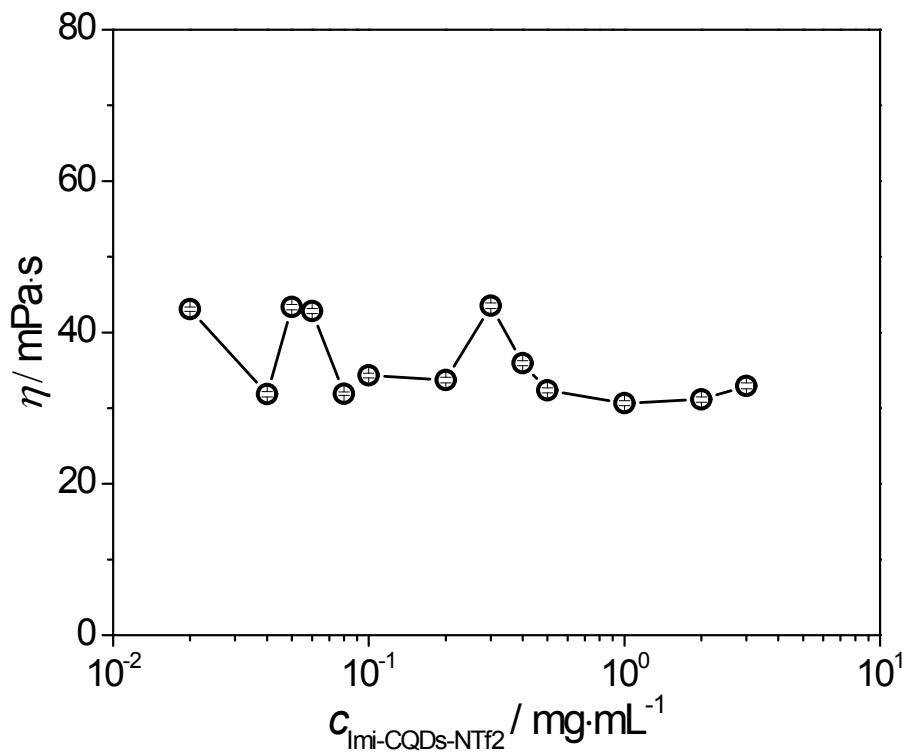


Fig. S16 Viscosity of Imi-CQDs-NTf₂/1a hybrid as a function of $c_{\text{Imi-CQDs-NTf}_2}$.

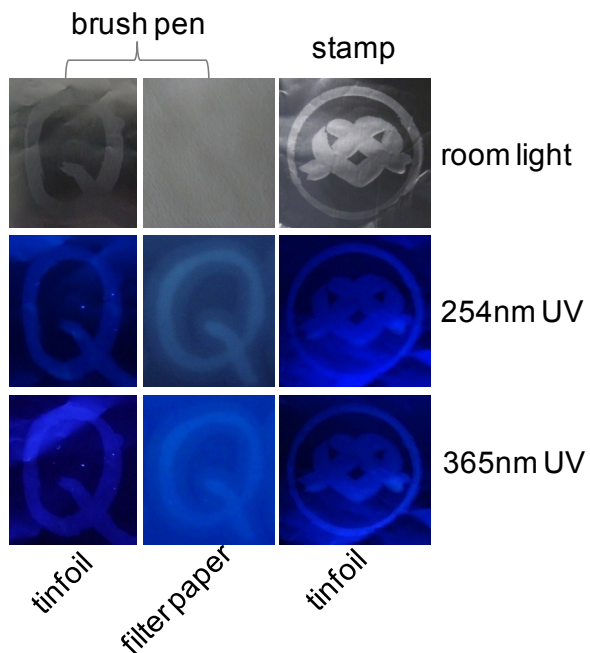


Fig. S17 The letter of *Q* written by the brush pen and the pattern templated by the stamp using Imi-CQDs-NTf₂/1a as the ink on tinfoil and filter paper under room light or UV irradiation, respectively.



Fig. S18 The letters of *CQDs* written by a gel ink pen on a silica plate after three cycles of immersing (20 min each) in an aqueous solution with pH=14 followed by total drying. Taken under irradiation at 365 nm by a portable UV lamp.

Table S1. Fluorescence quantum yield (Φ) as a function of the molar ratio of CA to [APMIm][Br] ($n_{\text{CA}}/n_{[\text{APMIm}][\text{Br}]}$), the temperature (T) and time (t) during pyrolysis. The amount of CA was fixed at 1.0 g.

T / °C	t / h	$n_{\text{CA}}/n_{[\text{APMIm}][\text{Br}]}$	Φ
240	2	1/1	6.16
240	2	1/3	11.37
240	2	1/5	6.28
210	2	1/3	6.11
270	2	1/3	1.51
240	1	1/3	8.59
240	3	1/3	7.39
240	4	1/3	8.03

Table S2. Parameters derived from time-resolved PL decay curves of an aqueous solution of as-prepared Imi-CQDs-Br in water ($0.5 \text{ mg}\cdot\text{mL}^{-1}$) at various emission wavelengths ($\lambda_{\text{ex}} = 377.8 \text{ nm}$).

$\lambda_{\text{em}} / \text{nm}$	Relaxation Time / ns		χ^2	Average Relaxation Time $\langle\tau\rangle^{\text{a}}$ / ns
	τ_1 / ns	τ_2 / ns		
400	1.55 (53.86%)	6.73 (46.14%)	1.305	3.94
420	1.80 (49.07%)	8.19 (50.93%)	1.256	5.05
440	2.02 (45.86%)	9.25 (54.14%)	1.201	5.93
460	2.17 (43.19%)	9.60 (56.91%)	1.160	6.41
480	2.22 (44.29%)	9.64 (55.71%)	1.221	6.35
500	2.24 (43.97%)	9.71 (56.03%)	1.229	6.43
520	2.34 (43.86%)	9.83 (56.14%)	1.202	6.54
540	2.29 (43.62%)	9.59 (56.38%)	1.253	6.41
560	2.33 (43.89%)	9.60 (56.11%)	1.176	6.41
580	2.23 (43.66%)	9.31 (56.34%)	1.244	6.22
600	2.10 (47.81%)	9.16 (52.19%)	1.083	5.78
620	2.06 (46.61%)	8.88 (53.39%)	1.156	5.70
640	1.99 (46.50%)	8.70 (53.50%)	1.083	5.58

^a $\langle\tau\rangle$ is calculated as follows: $\langle\tau\rangle = \tau_1 \times A_1 + \tau_2 \times A_2$

Table S3. The concentration of Imi-CQDs-NTf₂ in **1a** estimated by measuring the absorbance at $\lambda=300$ nm of the bottom phase. The relationship between concentration and absorbance can be fitted according to Lambert's law below the threshold concentration ($y=2.153x$).

$c_{\text{Imi-CQDs-Br}} / \text{mg}\cdot\text{mL}^{-1}$	Absorbance	$c_{\text{Imi-CQDs-NTf2}} / \text{mg}\cdot\text{mL}^{-1}$
0.02	0.05	0.02
0.04	0.096	0.04
0.05	0.103	0.05
0.06	0.119	0.06
0.08	0.179	0.08
0.10	0.178	0.10
0.2	0.368	0.17
0.3	0.538	0.25
0.4	0.674	0.31
0.5	0.735	0.34
1.0	1.212	0.56
2.0	1.862	0.86
3.0	1.999	0.93